Regional Carbon Emission Management Based on Probabilistic Power Flow With Correlated Stochastic Variables

Xu Wang, Yu Gong, and Chuanwen Jiang

***Abstract*—Most existing carbon emission management strategies only control the total carbon emission without focusing on both the regional carbon emission and the stochastic properties of the system. Correlated regional loads and unpredictable renewable energies in the power system make regional carbon emission management (RCEM) increasingly challenging and necessary. A complex multi-objective RCEM model based on probabilistic power flow (PPF) considering correlated variables is contributed in this paper. The three objective functions to be minimized are 1) the cost of electricity generated, 2) the total carbon emission, and 3) the carbon emission difference among regions which reflects the regional carbon emission imbalance from the supply side. A new clonal selection algorithm (CSA) coupled with a fuzzy satisfying decision method and an extended $2m + 1$ point estimate method (PEM) is proposed to solve this multi-objective RCEM model. The proposed method is illustrated through IEEE 30-bus, IEEE 118-bus and simplified Shanghai case studies. The proposed model can help reduce the total carbon emission, control regional carbon emission, prevent probabilistic congested lines from overloading, and choose the most suitable region for wind farms (WFs).**

***Index Terms*—Carbon flow tracing, multi-objective optimization, probabilistic power flow, regional carbon emission.**

I. Introduction

THE growing energy demand increases the greenhouse gas (GHG) emissions greatly, which has caused the earth to warm [1]. Worldwide, the electric power sector accounts for a rapid increasing percent of the total GHG emissions, which will pose a great threat to our human society. In addition, CO_2 contributes 77% of the total GHG effects [2]. Carbon emission management has attracted more global attentions currently.

Optimal dispatching with low-carbon sources and demand side management (DSM) are two main approaches to reduce the carbon emission. Essentially, DSM reduces the carbon emission level [3] through improving the energy efficiency and demand response [4]. Generally, frequently interactive DSM requires higher payouts than just rescheduling generation from the supply side.

Manuscript received February 14, 2014; revised June 03, 2014; accepted July 28, 2014. Date of publication August 18, 2014; date of current version February 17, 2015. This work was supported by the National High Technology Research and Development Program 863 of China (2012AA050204). Paper no. TPWRS-00220-2014

The authors are with the Key Laboratory of Control of Power Transmission and Conversion, Ministry of Education, Shanghai Jiao Tong University, Shanghai 200030, PR China (e-mail: wangx198912@163.com; gongyu200810@126.com; jiangcw@sjtu.edu.cn).

Digital Object Identifier 10.1109/TPWRS.2014.2344861

As a consequence, optimal dispatching with low-carbon sources is a better choice. The environmentally constrained optimal dispatch method has been thoroughly studied in recent years. A traditional low-carbon dispatch model combined with the impact of wind power was presented in [5]. In [6], [7], the environmentally constrained optimal dispatch model took the major operating characteristics of a CO_2 capture power plant into account. As its high 'efficiency penalty', an emission concerned wind-electric vehicle coordination dispatch model [8] was proposed. Also, wind power and coal-fired generation were coordinated in the day-ahead scheduling [9]. Though a useful tool in both fuel saving and carbon emission reduction, wind power increases the uncertainties of the power system. However, these researches just focus on the optimal dispatch under low-carbon economy, neglecting of other factors such as PPF and RCEM problems.

With China's huge investments in the low-carbon and sustainable energy, more highly stochastic and unpredictable system operating conditions will be imposed to system operators. PPF method, as a probabilistic analysis tool, is urgently needed. The PPF method was first proposed by Borkowska in 1974 [10]. Many papers [10]–[22] have been published in this interesting area. The discrete convolution technique, proposed in [22], is not only computationally intensive but performs badly in processing nonlinear problems. For nonlinear load flow equations, the computation burdens can be greatly relieved using PEM [13]–[16]. Actually, nodal powers within the same region may be correlated. The multivariate Gram-Charlier Type A series in [21] can be applied to solving this problem. Recently, the Gram-Charlier expansion has been widely used to estimate the probability density function (PDF) [18], [19]. However, this method produces probability distribution calculations greater than 1.00 and has serious convergence problems for non-Gaussian PDF, especially for wind power [23]. So the Cornish-Fisher expansion in [23], [24] is used in this paper.

This paper presents the concept of RCEM. The application of RCEM can balance the carbon emission in different regions with the total cost and carbon emission under control. Through RCEM, one region of a city can be prevented from over polluted, which may incur protests from citizens in that region and limit the dispersion of the pollutants. Only wind power is included in RECM for its typicality. Practically, RCEM problem is a multi-objective optimal PPF problem with correlated input random variables (IRVs). It can be divided into two parts, one is PPF with correlated IRVs and the other is multi-objective opti-

mization. For the first part, an extended $2m+1$ PEM [14]–[16] is applied for its best performance in processing correlated IRVs. For the second part, a novel CSA coupled with a fuzzy satisfying decision method is proposed. What's more, a carbon tracing model [26] is used to reveals the regional supply-demand imbalance which can guide the future grid planning in RCEM.

This paper is organized as follows. The mathematical formulations of RCEM are presented in Section II. Section III gives the PPF model coupled with correlated IRVs. In Section IV, the method to process uncertainties and correlations of the IRVs is proposed. Section V gives the CSA method coupled with a fuzzy satisfying decision method. Sections VI and VII provide two case studies. Finally, Section VIII provides the relevant conclusions.

II. Mathematical Formulations of RCEM

The RCEM is a multi-objective optimization problem balancing the relationships among the electricity generation cost, the total carbon emission and the regional carbon emission with the system constraints satisfied for one day. This section presents the multi-objective RCEM model.

A. Objective Function

The RCEM model is proposed at the average load level for one day and includes three minimum objective functions presented as follows.

1) Electricity generation cost in a day:

$$\overline{f}_1 = \sum_{i=1}^{N_{TPG}} C_{TPG,i}(\overline{P}_{TPG,i}) + \sum_{j=1}^{N_{WFs}} C_{WFs,j}(\overline{P}_{WFs,j}) \quad (1)$$

where N_{TPG} is the number of the traditional power generators (TPGs), $C_{TPG,i}(\cdot)$ is the cost function of TPG i, $\overline{P}_{TPG,i}$ is the expected active power generated by TPG i, N_{WFs} is the number of the buses with WFs, $C_{WFs,j}(\cdot)$ is the cost function of bus j with WFs, and $\overline{P}_{WFs,j}$ is the expected active power generated by bus j with WFs.

2) Total carbon emission produced in a day:

$$\overline{f}_2 = \sum_{i=1}^{N_{TPG}} \overline{E}_{TPG,i} + \sum_{j=1}^{N_{WFs}} \overline{E}_{WFs,j} \quad (2)$$

where $\overline{E}_{TPG,i}$ is the expected carbon emission produced by TPG i, and $\overline{E}_{WFs,j}$ is the expected carbon emission produced by bus j with WFs.

3) Carbon emission difference among regions in a day:

$$\overline{f}_3 = \sum_{i=1}^{N_{reg}-1} \sum_{j=i+1}^{N_{reg}} \left|\overline{E}_i - \overline{E}_j\right| \quad (3)$$

where N_{reg} is the number of regions, $\overline{E}_i$ and $\overline{E}_j$ are the expected carbon emission in region i and j, respectively. This is an index reflecting the carbon emission imbalance. The lower the index, the more balanced the carbon emission in each region is. The higher the index, the more serious some region is polluted.

B. Constrains and Limits

1) Power flow equations:

$$\begin{cases} P_i = V_i \sum\limits_{j=1}^{N_{bus}} V_j(G_{ij}\cos\theta_{ij} + B_{ij}\sin\theta_{ij}) \\ Q_i = V_i \sum\limits_{j=1}^{N_{bus}} V_j(G_{ij}\sin\theta_{ij} - B_{ij}\cos\theta_{ij}) \end{cases} \quad (4)$$

where P_i, Q_i and V_i are the active power, reactive power and voltage amplitude of bus i, respectively; N_{bus} is the number of buses; θ_{ij} is the phase angle difference between bus i and j; G_{ij} and B_{ij} are conductance and susceptance between bus i and j.

2) Power constraints of TPGs:

$$\begin{cases} P_{TPG_i}^{\min} \le P_{TPG_i} \le P_{TPG_i}^{\max} \\ Q_{TPG_i}^{\min} \le Q_{TPG_i} \le Q_{TPG_i}^{\max} \end{cases} \quad (5)$$

where $P_{TPG_i}^{\min}$ and $P_{TPG_i}^{\max}$ are the minimum and maximum active power of TPG i; $Q_{TPG_i}^{\min}$ and $Q_{TPG_i}^{\max}$ are the minimum and maximum reactive power of TPG i; P_{TPGi} and Q_{TPGi} are the active and reactive power of TPG i.

3) Bus voltage limits:

$$Pro(V_i^{\min} \le V_i \le V_i^{\max}) \ge \alpha_i, \quad i = 1, 2, \ldots, N_{bus} \quad (6)$$

where $Pro(\cdot)$ denotes the probability of the event $(\cdot)$; $V_i^{\min}$ and $V_i^{\max}$ are the lower and upper bound of voltage amplitude of bus i; V_i is the voltage amplitude of bus i; α_i is the confidence level of the bus i's constraint.

4) Line power flow limits:

$$Pro(|Pf_i| \le Pf_i^{\max}) \ge \beta_i, \quad i = 1, 2, \ldots N_{branch} \quad (7)$$

where $Pf_i^{\max}$ are the upper limit of transmission power of branch i; Pf_i is the power flow of branch i; β_i is the confidence level of the branch i's constraint; N_{branch} is the number of the branches.

In the above formulas, the superscript '$-$' denotes the expectation of the random variables. The RCEM model is proposed for one period, such as a day or a week. Moreover, it can also solve the RCEM problem in several periods through summing up the objective functions in different periods and adding together ramping constraint of generators which is an chance constraint similar to (6) and (7). This chance constraint is omitted for only one period is studied in this paper.

III. Probabilistic Power Flow

A. Overview

Mathematically, the power flow problem [10]–[24], determining the operation conditions of a power system, is:

$$s = G(p) \quad (8)$$

where s is the vector of output variables calculated through the power flow function $G(\cdot)$, and p is the vector of input variables representing the power injection at every bus except for

the slack. The power flow problem becomes a PPF problem accounting for the inherent uncertainty of the input vector p.

B. $2m+1$ PEM

$2m+1$ PEM provides the best performance in processing a high number of IRVs, both continuous and discrete, among different PEMs [15], [16]. Moreover, the $2m+1$ PEM can also process correlated IRVs [14]. Considering there are m IRVs and n output random variables in the system, (8) can be rewritten as:

$$s_i = G_i(p_1, p_2, \ldots, p_m), \quad i = 1, 2, \ldots, n \tag{9}$$

where $s = [s_1, s_2, \ldots, s_n]$ and $s = [p_1, p_2, \ldots, p_m]$. The first four central moments of p_l is used to approximate to the PDF of s_i by three points. Each point is a pair $(p_{l,k}, \omega_{l,k})$ with $k = 1$, 2, 3, composed of a location $p_{l,k}$ where the corresponding $s_{l,k}$ is to be estimated and a weighting factor $\omega_{l,k}$ which measures the impact of this estimation on the random behavior of s_i. The locations $p_{l,k}$ can be calculated by:

$$p_{l,k} = \mu_{p_l} + \xi_{l,k} \cdot \sigma_{p_l}, \quad k = 1, 2, 3 \tag{10}$$

where μ_{p_l} and σ_{p_l} are the mean and standard deviation of p_l, and $\xi_{l,k}$ is the standard location given by [14]:

$$\xi_{l,k} = \frac{\lambda_{p_l,3}}{2} + (-1)^{3-k}\sqrt{\lambda_{p_l,4} - \frac{3}{4}\lambda_{p_l,3}^2},\ k = 1, 2;\ \xi_{l,3} = 0. \tag{11}$$

The parameters $\lambda_{p_l,3}$ and $\lambda_{p_l,4}$ are the coefficients of skewness and kurtosis of p_l, and can be computed as:

$$\lambda_{p_l,j} = \int_{-\infty}^{+\infty} \frac{(p_l - \mu_{p_l})^j f_{p_l} dp_l}{{\sigma_{p_l}}^j}, \quad j = 3, 4. \tag{12}$$

For each location $p_{l,k}$, the corresponding weighting factor $\omega_{l,k}$ are expressed as [14], [15]:

$$\omega_{l,k} = \frac{(-1)^{3-k}}{\xi_{l,k}(\xi_{l,1} - \xi_{l,2})},\ k = 1, 2; \quad \omega_{l,3} = \frac{1}{m} - \frac{1}{\lambda_{l,4} - \lambda_{l,3}^2}. \tag{13}$$

For each pair $(p_{l,k}, \omega_{l,k})$, the ith component of the solution vector of the power flow estimation is calculated as follows:

$$s_i(l,k) = G_i(\mu_{p_1}, \mu_{p_2}, \ldots, p_{l,k}, \ldots, \mu_{p_m}), \quad l = 1, 2, \ldots m;\ k = 1, 2. \tag{14}$$

Then, the jth raw moment of s_i can be estimated as [14]:

$$E(s_i^j) \approx \sum_{k=1}^{3}\sum_{l=1}^{m}\left[\omega_{l,k} \cdot s_i^j(l,k)\right], \quad j = 1, 2, \ldots \tag{15}$$

where $E(\cdot)$ stands for the expectation operator. Note that the third location of $p_{l,3}$ exactly equal to its mean μ_{pl} according to (11). Then (15) is modified to:

$$E(s_i^j) \approx \sum_{k=1}^{2}\sum_{l=1}^{m}\left[\omega_{l,k} \cdot s_i^j(l,k)\right] + G_i^j(\mu_{p_1}, \mu_{p_2}, \ldots, \mu_{p_m}) \cdot \sum_{l=1}^{m}\omega_{l,3}, \quad j = 1, 2, \ldots. \tag{16}$$

The deterministic power flow of a system with m IRVs needs to be calculated for $2m+1$ times. So it is called $2m+1$ PEM.

C. Cornish-Fisher Expansion

All the moments of a random variable obtained through the above $2m+1$ PEM can be used to approximate its PDF accurately through Cornish-Fisher expansion [23], [24], which is related but superior to Gram-Charlier expansion. However, Cornish-Fisher expansion has two pitfalls: one is exceeding the domain of validity of the expansion and the other is confusing the skewness and kurtosis parameters of the calculated results with the actual ones [34]. In Section VI-B, it is proved that the data used are within the domain of validity of the Cornish-Fisher expansion and the impacts of the errors of the skewness and kurtosis parameters on the approximate are quite small. So these two pitfalls are avoided. The theoretical deduction of Cornish-Fisher expansion can refer to [25].

Using the first five cumulants, the s_i can be computed as:

$$\begin{aligned} S_i(\alpha) \approx{}& \Phi^{-1}(\alpha) + \frac{1}{6}\left(\Phi^{-1}(\alpha)^2 - 1\right)\kappa_3 \\ &+ \frac{1}{24}\left(\Phi^{-1}(\alpha)^3 - 3\Phi^{-1}(\alpha)\right)\kappa_4 \\ &- \frac{1}{36}\left(2\Phi^{-1}(\alpha)^3 - 5\Phi^{-1}(\alpha)\right)\kappa_3^2 \\ &+ \frac{1}{120}\left(\Phi^{-1}(\alpha)^4 - 6\Phi^{-1}(\alpha)^2 + 3\right)\kappa_5 \\ &- \frac{1}{24}\left(\Phi^{-1}(\alpha)^4 - 5\Phi^{-1}(\alpha)^2\right)\kappa_2\kappa_3 \\ &+ \frac{1}{324}\left(12\Phi^{-1}(\alpha)^4 - 53\Phi^{-1}(\alpha)^2\right)\kappa_3^3 \\ s_i ={}& S_i \cdot \sigma_{s_i} + \mu_{s_i} \end{aligned} \tag{17}$$

where $\Phi(\cdot)$ are the CDF of standard normal distribution; μ_{s_i} and σ_{s_i} are the mean and standard deviation of s_i; κ_j is the jth order cumulant of s_i which can refer to formula (12) in [23]. The accuracy of this method regarding to the Monte Carlo method is demonstrated in Section VI-B.

IV. Uncertainties and Correlations Processing

To simulate the uncertainties of the IRVs, such as loads and wind power, probabilistic models are established. As the correlations among IRVs significantly affects the power flows [14], [28], an improved $2m+1$ PEM capable of managing the correlations, is introduced.

A. Probabilistic Correlated WFs Model

The output of WFs at bus t depends on the wind speed generally considered to follow the Weibull distribution. Under the assumption that the joint moments over than 2nd order are zero, the joint output of the correlated WFs at bus t can be obtained through the correlated wind speed.

The correlated wind speeds $V = [v_1, v_2, \ldots, v_{N_{WFs,t}}]$ of the $N_{WFs,t}$ WFs at bus t can be generated via the method as follows:

1. Generate a matrix of $N_{WFs,t}$ independent standard normal distributed random variables $R_{N_s \times N_{WFs,t}} = [r_1, r_2, \ldots, r_{N_{WFs,t}}]$ (N_s represents the sampling times).
2. For the desired correlation coefficient matrix C_d of the wind speeds, the modified correlation coefficient matrix C_{md} by the Nataf transformation [20] are obtained using the Formula (22) and (23) in [14]. Then decompose C_{md}

by the Cholesky decomposition method [14] into $C_{md} = LL^T$.

3. Using the transformation $Y = LR$ and the inverse Nataf transformation $v_j = F_j^{-1}(\Phi(Y))$, the final sampling matrix $V_{N_s \times N_{WFs,t}} = [v_1, v_2, \ldots, v_{N_{WFs,t}}]$ with $N_{WFs,t}$ Weibull distributed variables and correlation coefficient matrix C_d is obtained.

The wind speed vector v_j from the jth column of V determines the output column vector $P_{WF,j}[N_s \times 1]$ of WF j with n_j wind turbine generators (WTGs) at the bus t:

$$P_{WF,j}(v_j) = \begin{cases} 0 & v_j < v_{in} \\ n_j P_r \frac{(v_j - v_{in})}{(v_r - v_{in})} & v_{in} \le v_j \le v_r \\ n_j P_r & v_r < v_j \le v_{out} \\ 0 & v_j > v_{out} \end{cases} \tag{18}$$

where P_r is the rated power of a single WTG; v_{in}, v_r and v_{out} are the cut-in, rated and cut-out wind speed, respectively.

Then, the output sampling matrix $P_{WFs}[N_s \times 1]$ is obtained by:

$$P_{WFs} = \sum_{j=1}^{N_{WFs,t}} P_{WF,j}. \tag{19}$$

The mean and standard deviation of WFs' output can be calculated by:

$$\begin{cases} \mu_{WFs,t} = \dfrac{\sum_{i=1}^{N_s} P_{WFs}(i)}{N_s} \\ \sigma_{WFs,t} = \sqrt{\dfrac{\sum_{i=1}^{N_s} [P_{WFs}(i) - \mu_{WFs,t}]^2}{N_s}} \end{cases} \tag{20}$$

where $P_{WFs}(i)$ is the ith element of P_{WFs}. The zth ($z > 2$) order standardized central moments of the bus t with WFs can be calculated as:

$$M_{z,t} = \frac{\left(\frac{1}{N_s} \sum_{i=1}^{N_s} [P_{WFs}(i) - \mu_{WFs,t}]^z \right)}{\sigma_{WFs,t}^z}. \tag{21}$$

No matter the IRVs are continuous or discrete, the $2m + 1$ PEM can be just applied to the uncorrelated ones. Thus, Part B introduces a modified $2m + 1$ PEM to process correlated IRVs.

B. $2m + 1$ PEM for Correlated IRVs

[33] processed the correlated IRVs by using joint moments and joint cumulants. But the joint PDF of the correlated IRVs is required, which is hardly obtained in practical engineering. For this reason, the orthogonal transformation [14] based on Cholesky decomposition [17] is used to approximate the PPF with correlated IRVs. The $2m + 1$ PEM for correlated IRVs p is as follows:

1. Obtain the matrix B by Cholesky decomposition using $C_p = LL^T$ and $B = L^{-1}$, where C_p is the variance-covariance matrix.
2. Transform the correlated IRVs p into a new set of independent variables q whose first four central moments satisfy the following equations (under the assumption that the joint moments of an order higher than two are zero):

$$\begin{aligned} \mu_q &= B\mu_p; \quad \sigma_q^2 = I_m; \\ \lambda_{q_l,j} &= \sum_{i=1}^{m} (b_{li})^j \lambda_{p_l,j} \sigma_{p_l}^j, \; j = 3, 4 \end{aligned} \tag{22}$$

where μ_p and μ_q are the mean vectors of p and q; σ_p and σ_q are the standard deviation vectors of p and q; I_m is the m-dimensional identity matrix; $\lambda_{q_l,j}$ (j = 3,4) are the coefficients of skewness and kurtosis of q_l; b_{li} is the lth row and ith column element of B.

3. Calculate the new transformed pairs $(q_{l,k}, \omega_{l,k})$ of independent q defining the new $2m + 1$ PEM using (10)–(13).
4. Construct the new $2m + 1$ points in the form $(\mu_{q_1}, \ldots, q_{l,k}, \ldots, \mu_{q_m})$ and $(\mu_{q_1}, \ldots, \mu_{q_l}, \ldots, \mu_{q_m})$. Let $q_{2m+1,k}$, k = 1,2,3, be a $m \times m$ matrix each row of which is one point of the $2m + 1$ points with l from 1 to m. Then transform the $2m + 1$ points to the original space by $p_{2m+1,k} = B^{-1} q_{2m+1,k}$.
5. Calculate the deterministic power flow using (14) for each row of $p_{2m+1,k}$ for $2m + 1$ times. This step yields the solution vectors $s_i(l, k)$.
6. Estimate the the jth raw moment, PDF and CDF of s_i.

V. Solution Methodology

Firstly, the CSA with hybrid variation strategy is implemented to solve the multi-objective RCEM model. Then the interactive fuzzy satisfying method is used to convert the objective functions into a min-max problem.

A. CSA

The CSA in [29] has never been implemented in power engineering. Compared with the standard genetic algorithm, the CSA can reach a diverse set of local optima solutions while genetic algorithm tends to polarize towards local optima solution. Thus, the multi-objective CSA using hybrid variation strategy is adopted. The detailed procedure is as follows:

Step 1: Read the input data.

Step 2: Generate initial populations with the ith antibody satisfying the constraint (5):

$$\begin{aligned} X_i &= [x_{i1}, \ldots, x_{ij}, \ldots, x_{iN_{dv}}] \\ &\quad i = 1, 2, \ldots, N_{pop}; \; j = 1, 2, \ldots, N_{dv} \end{aligned} \tag{23}$$

where x_{ij} is the jth element of X_i; N_{pop} is the size of the populations; N_{dv} is the number of decision variables.

Step 3: Each antibody is cloned $N_{cl,\max}$ times using hybrid variation strategy to update the populations.

1) The mutation rate and the mutation elements scale of every cloning operation is determined by:

$$\begin{aligned} r(N_{Iter}) &= r_{\max} - (r_{\max} - r_{\min}) \cdot \frac{N_{Iter}}{N_{Iter,\max}} \\ N_{Scale} &= round\,[r(N_{Iter}) \cdot N_{dv}] \end{aligned} \tag{24}$$

where N_{Iter} is the current iteration; $N_{Iter,\max}$ is the maximum number of the iterations; $r(N_{Iter})$, $r_{\max}$

and $r_{\min}$ are the current, maximum and minimum mutation rate; N_{Scale} is the number of the mutation elements in the current antibody; $round(\cdot)$ denotes the rounding operation.

2) If the current cloning number $N_{cl} < 0.8N_{cl,\max}$, random step mutation is applied:

$$x_{ij}^{new} = x_{ij} + (-1)^y step_r D_r$$
$$D_r = \begin{cases} x_{ij}^{\max} - x_{ij}, & y\%2 = 1 \\ x_{ij} - x_{ij}^{\min}, & y\%2 = 0 \end{cases}. \quad (25)$$

Otherwise, fixed step mutation is adopted:

$$x_{ij}^{new} = x_{ij} + (-1)^y step_f D_f$$
$$step_f = 0.05 \cdot \left(1 - \frac{N_{Iter}}{N_{Iter,\max}}\right)$$
$$D_f = x_{ij}^{\max} - x_{ij}^{\min} \quad (26)$$

where y is a random integer; $step_r$ is a random step following uniform distribution on the interval [0, 1]; $x_{ij}^{\max}$ and $x_{ij}^{\min}$ are the upper and lower limits of the jth decision variable of the ith antibody; $step_f$ is a fixed step; % denotes the operation of reminder calculation.

Step 4: Adjust the new antibodies to satisfy the constraint (5) and compute PPF. Then check the chance constraints (6) and (7) by calculating the penalty terms:

$$Pen\_V = \sum_{i=1}^{N_{bus}} \left| \frac{\Delta V_i}{V_i^{\max} - V_i^{\min}} \right|, \quad Pen\_P = \sum_{i=1}^{N_{line}} \left| \frac{\Delta P_i}{P_i^{\max}} \right| \quad (27)$$

where ΔV_i and ΔP_i are computed by:

$$\Delta V_i = \begin{cases} 0, & \text{(6) satisfied} \\ \max\left\{V_i^{\min} - V_i^{down}, V_i^{up} - V_i^{\max}\right\}, & \text{else} \end{cases}$$
$$\Delta P_i = \begin{cases} 0, & \text{(7) satisfied} \\ P_i^{up} - P_i^{\max}, & \text{else} \end{cases} \quad (28)$$

where $Pro\left(V_i < V_i^{down}\right) = 1 - \alpha_i$; $Pro\left(V_i > V_i^{up}\right) = 1 - \alpha_i$; $Pro\left(|P_i| > P_i^{up}\right) = 1 - \beta_i$.

Step 5: Modify the original objective functions $\overline{f}_i$ into the new objective functions $\overline{f}_i^{new}$:

$$\overline{f}_i^{new} = \overline{f}_i + w_{V,i} Pen\_V + w_{P,i} Pen\_P, \quad i = 1, 2, 3 \quad (29)$$

where $w_{V,i}$ and $w_{P,i}$ are the penalty factors.

Step 6: Calculate the new objective functions using (28) for each antibody and obtain the Pareto-optimal set through selecting the antibodies using the Pareto dominant theory.

Step 7: Check the current size of the Pareto-optimal set. If the current size is larger than the allowed one N_{Pas}, eliminate the antibodies from the Pareto-optimal set as follows:

1) Sort the antibodies in ascending order according to $\overline{f}_1$.
2) Save the two antibodies which have the maximum and minimum value $\overline{f}_1^{\max}$ and $\overline{f}_1^{\min}$. Then calculate the fitness of others:

$$fitness(X_i) = \frac{\overline{f}_1(X_{i+1}) - \overline{f}_1(X_{i-1})}{\overline{f}_1^{\max} - \overline{f}_1^{\min}}, \quad i = 2, 3, \ldots, N_{Pas} - 1. \quad (30)$$

3) Eliminate the antibody having the smallest fitness until the size of the Pareto-optimal set is reduced to N_{Pas}.

Step 8: Update the Pareto-optimal set.

Step 9: Verify the termination criterion. If $N_{Iter} < N_{Iter,\max}$, go back to Step 3; otherwise, stop the optimization search and output the optimal solutions.

B. Fuzzy Satisfying Decision Making

To select the 'best' compromised solution, interactive fuzzy satisfying method [30] based on Logistic membership function (LMF) is used. Each objective function is modeled by:

$$L_{\overline{f}_i}(X_i) = \frac{1}{1 + e^{\varepsilon_i \cdot \left(U[\overline{f}_i(X_i)] - \chi_i\right)}}, \quad i = 1, 2, 3 \quad (31)$$

where $U(\cdot)$ is a linear normalization function; ε_i and χ_i are the parameters of LMF which determines the fuzzy value and the intermediate point for $\overline{f}_i$, and here $\varepsilon_i = 10$, $\chi_i = 0.5$.

A particular optimal solution based on the preference of the decision maker is obtained through solving the following min-max problem:

$$\min_{X_i \in \Omega} \left\{ \max \left\{ \left| L_{wi} - L_{\overline{f}_i}(X_i) \right| \right\} \right\}, \quad i = 1, 2, 3 \quad (32)$$

where Ω is the Pareto-optimal set; L_{wi} is the ith reference membership value which is a real number in the range of [0,1] and higher value represents the corresponding objective function is more important.

VI. IEEE 30-Bus Case Study

The RCEM model is solved for the modified IEEE 30-bus power system [31], [32] in detail, which consists of 6 generators, 41 branches, 20 loads and 3 regions. The studies have been implemented in MATLAB 2012a.

Assumptions

1) Generators and Loads Data: Fig. 1 and Table I show the locations and detailed generator data [32] used in this paper. The active power consumption of each load is assumed to be normally distributed with means equal to the values provided in [31, Table III] with the value at bus 5 zeroed out (the largest load in the system makes it difficult to satisfy the chance constraints). The test is applied at an average load level for a day 24 hours. So the standard deviation of each load is set to 20% of its corresponding mean value. The rated capacities of branches are raised to 1.5 times of the original ones. For calculation convenience, the power factor of each load computed from the load data is kept constant.

2) WFs' Data: All the wind speed data used are considered to follow the Weibull distribution with scale and shape parameters 8.5, 2.75, respectively. Fig. 2 depicts the mean μ and standard deviation σ of the output of two 15-MW WFs composed by five 3-MW WTGs as Table II shows with the correlation coefficient increasing from 0 to 1. From Fig. 2, the correlations of the wind speeds significantly affect the statistical performance of WFs. WFs have the same expected output when they are independent or completely correlated. Here, if a bus is integrated with WFs, the WFs are assumed to be two 15-MW ones composed by five SL3000 WTGs with a correlation coefficient of 0.9 and a power

TABLE I
GENERATOR DATA

Bus No.	P_G^{max} [MW]	P_G^{min} [MW]	Q_G^{max} [MVar]	Q_G^{min} [MVar]	Cost coefficients			Carbon intensity [t/MWh]
					a [$/h]	b [$/MWh]	c [$/MW^{2}h]	
1	80	0	150	-20	0	2.0	0.02	1.186
2	80	0	60	-20	0	1.75	0.0175	1.186
13	40	0	44.7	-15	0	3.0	0.025	0.78
22	50	0	62.5	-15	0	1.0	0.0625	1.186
23	30	0	40	-10	0	3.0	0.025	0.434
27	55	0	48.7	-15	0	3.25	0.00834	0.434

Generating cost $C_i = a_i + b_i P_{Gi} + c_i P_{Gi}^2$

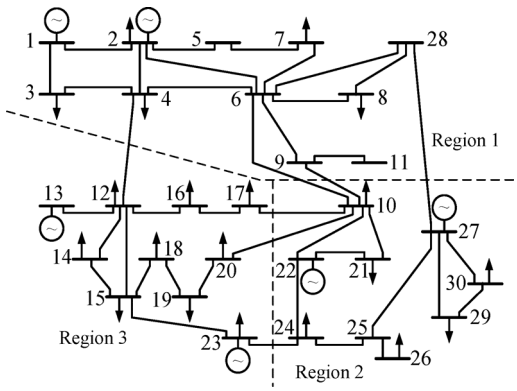

Fig. 1. IEEE 30-bus system.

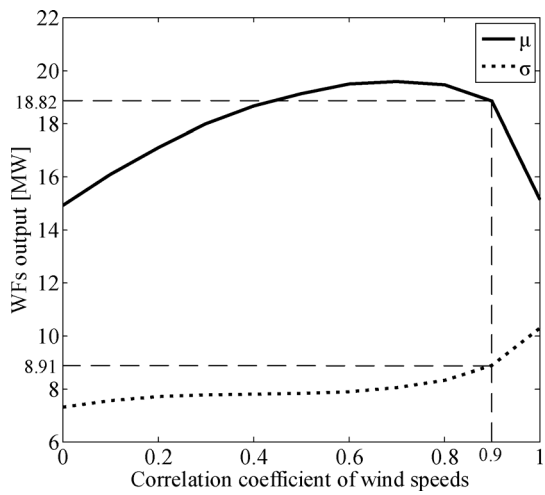

Fig. 2. Correlation effect on the WFs' output.

TABLE II
SL3000 WTG DATA

Cut in speed [m/s]	Rated speed [m/s]	Cut out speed [m/s]	Rated power [MW]	Rotor diameter [m]
3	12	25	3	113

factor 0.9 lagging. More wind power leads to more stringent constraints which will not be conducive to the case study.

3) Correlations and Parameters Set: Three regions are distinguished shown in Fig. 1. Correlations among buses are listed in Table III. The anti-load characteristics of WFs are considered using a negative correlation coefficient. As is accepted unconditionally, wind power is considered to be negative load. So

TABLE III
CORRELATION COEFFICIENT DATA BETWEEN TWO BUSES

Location of the two buses	Bus type	Load	Wind farms
In the same region	Load	0.8	-0.5
	Wind farms	-0.5	0.7
In the different regions	Load	0.2	-0.3
	Wind farms	-0.3	0.4

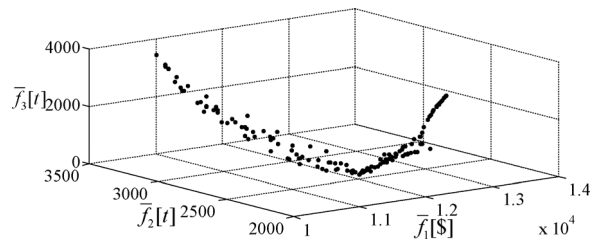

Fig. 3. The optimal front set of the objective functions (Case 1).

the correlation matrix of the buses is positive definite. The parameters of the CSA and the penalty factors are set as $N_{dv} = 12$, $N_{pop,initial} = 100$, $N_{pop,\max} = 150$, $N_{cl,\max} = 15$, $N_{Iter,\max} = 30$, $r_{\max} = 0.85$, $r_{\min} = 0.25$, $w_{V,1} = 3000$, $w_{P,1} = 2000$, $w_{V,2} = 1000$, $w_{P,2} = 6000$, $w_{V,3} = 100$, $w_{P,3} = 1000$.

A. Application of CSA

The CSA associated with the $2m + 1$ PEM is applied under different conditions including changing the confidential levels, the reference membership values and the WFs' locations. For these comparative purposes, three cases are applied, namely:

Case 1: WFs are located at bus 11 and 5.
Case 2: WFs are located at bus 11 and 13.
Case 3: WFs are located at bus 11 and 25.

Fig. 3 shows the optimal front set under confidential level $\alpha_i = \beta_i = 0.95$, Case 1. The figure indicates that it costs more to reduce total carbon emission. Also, we must pay more to decrease $\overline{f}_3[t]$ with the total carbon emission unchanged. The large range of the solution set provides lots of options for decision makers.

1) Accuracy of Cornish-Fisher Expansion: To verify the accuracy and viability of Cornish-Fisher expansion, its results are compared to those from Monte Carlo method and Gram-Charlier expansion. Cornish-Fisher expansion, with an equivalent computation times as Gram-Charlier, has fewer computation times than Monte Carlo method [19]. Fig. 4 shows the CDF curves of the power flow in branch 6–8 obtained by the three methods in Case 1. In the figure, the curve obtained

TABLE IV
OPTIMIZATION RESULTS UNDER DIFFERENT CONFIDENTIAL LEVELS ($L_{wi} = 1$, $i = 1,2,3$, CASE 1)

α_i=β_i	Active power outputs of TPGs [p. u.]						Objective functions			Regional carbon emission [t]		
	P_1	P_2	P_{13}	P_{22}	P_{23}	P_{27}	$\overline{f}_1$ [\$]	$\overline{f}_2$ [t]	$\overline{f}_3$ [t]	Region 1	Region 2	Region 3
0.95	0.0025	0.3465	0.8401	0.1633	0.9982	0.9998	12477.7572	2540.7359	292.7264	794.6253	805.1221	940.9885
0.98	0.2657	0.0798	0.8452	0.1644	0.9999	0.9999	12548.5441	2539.0679	316.9370	786.8981	806.8033	945.3665
1.00	0.0270	0.1063	0.8207	0.5208	0.9954	0.9997	13856.2764	2542.9686	2020.9719	303.4441	1313.9301	925.5943

TABLE V
DECISION RESULTS UNDER DIFFERENT REFERENCE MEMBERSHIP VALUES ($\alpha = \beta = 0.95$, CASE 1)

Reference membership value			Objective functions			Regional carbon emission [t]		
L_{w1}	L_{w2}	L_{w3}	$\overline{f}_1$ [\$]	$\overline{f}_2$ [t]	$\overline{f}_3$ [t]	Region 1	Region 2	Region 3
1	1	1	12477.7572	2540.7359	292.7264	794.6253	805.1221	940.9885
0.5	1	1	12573.5620	2511.5794	571.0971	712.5920	800.8470	998.1405
1	0.5	1	12105.5338	2596.3812	67.2177	874.2828	877.8536	844.2448
1	1	0.5	12428.4243	2530.9589	666.8409	622.4273	952.6839	955.8478
0.1	1	1	12864.2376	2486.2573	676.5352	714.0885	719.8127	1052.3561
1	0.1	1	11827.8608	2623.3609	383.6147	983.3963	848.3756	791.5890
1	1	0.1	12702.4098	2507.3249	1048.9040	493.2847	1017.7367	996.3035

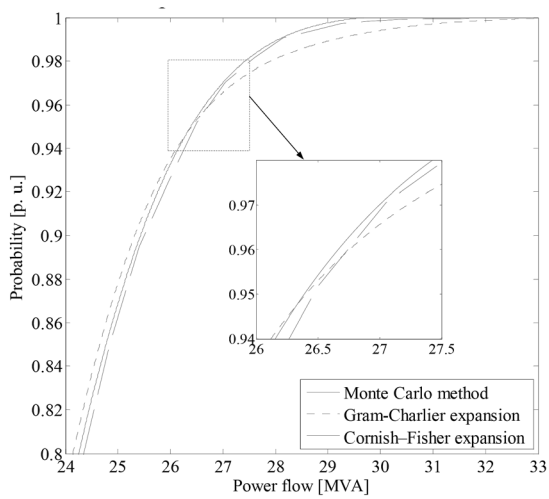

Fig. 4. CDF of power flow in branch 6–8 (Case 1).

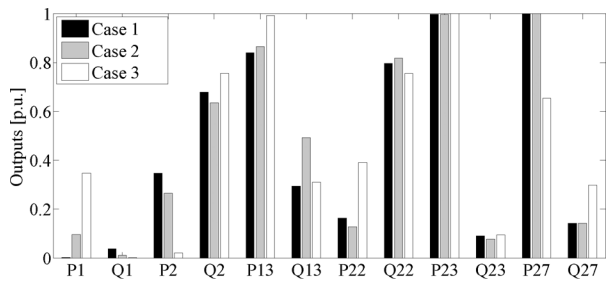

Fig. 5. Outputs of generators in different cases ($\alpha_i = \beta_i = 0.95$, $L_{wi} = 1$, $i = 1,2,3$).

by Cornish-Fish expansion is closer to the real distribution than Gram-Charlier and the largest relative error is less than 1.25% in the interval [0.8, 1] (The confidential level of the chance constraints is greater than 0.95). Obviously, the two pitfalls mentioned in Section III.C are avoided. Cornish-Fisher expansion is more suitable for the system containing the non-Gaussian PDF of the wind power, instead of Gram-Charlier expansion.

2) Effect of the Confidential Levels: Table IV lists the expected outputs of the TPGs and region carbon emission under different confidential levels. Higher confidential level leads to higher values of objective functions because higher confidential level means more stringent constraints which decrease feasible solutions. For example, when $\alpha_i = \beta_i = 1$, the outputs of P_{22} and P_{23} are limited as a result of branch limits so the objective functions have an obvious increase.

3) Effect of the Reference Membership Value: The reference membership values were set 1 to give equal weight to all the objective functions in the previous study. However, problems with non-commensurable objectives always arise. The effect of the reference membership values on decision results are shown in Table V. From the table, when f_1 and f_2 have the same degree of attention, these two objectives increase few with more attention paid to f_3. It indicates that we can decrease f_3 with f_1 and f_2 under nearly the same level. Also, Table V can help decision makers select a compromised solution or the most satisfactory plan based on their preference.

4) Effect of the WFs Locations: Three cases mentioned above are studied under confidential level $\alpha_i = \beta_i = 0.95$ with equal weight to all the objective functions to reveal the effects of the WFs' locations. Fig. 5 and Table VI provide the optimization results of the 30-bus system using Case 1, Case 2 and Case 3, respectively. According to the results, Case 1 has the best performance in the expected objectives and network losses from the supply side, especially in $\overline{f}_3$[t]. As the TPGs in Region 1 have higher average carbon intensity than the others, adding the WFs to Region 1 can balance regional carbon emission more properly than adding it to the other two. Also, the TPGs with higher carbon intensity (P_1, P_2, P_{22}) are rarely dispatched and WTGs can somehow increase the output of the TPGs with lower cost in the same region from Fig. 5.

B. Regional Carbon Emission Assessment

All the cases have been studied from the power supply side. Most of the time, it is difficult to select the best plan just from

TABLE VI
OPTIMIZATION RESULTS OF 30-BUS SYSTEM UNDER DIFFERENT CASES ($L_{wi} = 1$, $i = 1,2,3$, $\alpha = \beta = 0.95$)

Case	Objective functions			Regional carbon emission [t]			Average network losses per hour	
	$\overline{f}_1$ [$]	$\overline{f}_2$ [t]	$\overline{f}_3$ [t]	Region 1	Region 2	Region 3	Active power [MW]	Reactive power [MVAR]
1	12477.7572	2540.7359	292.7264	794.6253	805.1221	940.9885	2.8185	25.1026
2	12498.6807	2542.8969	410.6690	828.8538	754.3543	959.6888	2.8963	28.8116
3	12392.9648	2824.1100	431.5816	838.3945	931.5303	1054.1852	2.8631	25.6670

TABLE VII
CARBON INTENSITY ACCOUNTED FROM THE SUPPLY SIDE AND THE DEMAND SIDE

Region	Load [MW]	Outputs of TPGs [MW]			Carbon Intensity = Carbon emission/(24·Load) [t/MWh]					
					Supply side			Demand side		
		Case 1	Case 2	Case 3	Case 1	Case 2	Case 3	Case 1	Case 2	Case 3
1	84.5	27.9169	29.1194	29.4546	0.3918	0.4087	0.4134	0.5903	0.7130	0.7147
2	48.5	63.1519	61.3652	55.5009	0.6917	0.6481	0.6993	0.7601	0.8623	0.5952
3	56.2	63.5497	64.5217	69.6076	0.6976	0.7115	0.6310	0.3410	0.0755	0.5104
Total	189.2	154.6184	155.0063	154.6631	0.5595	0.5600	0.6219	0.5598	0.5619	0.6234

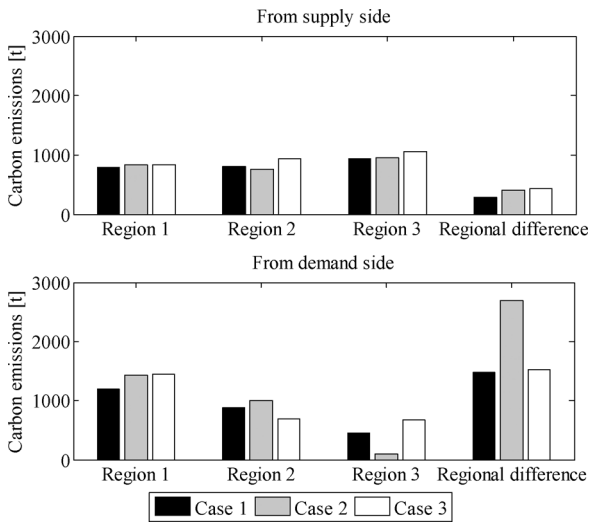

Fig. 6. Expected carbon emission of 30-bus system at each region.

TABLE VIII
CARBON INTENSITY DATA FOR GENERATORS OF DIFFERENT CAPACITIES

Capacity P [MW]	Carbon intensity [t/MWh]
$300 \le P < 600$	0.82155
$200 \le P < 300$	0.84914
$100 \le P < 200$	0.86835
$P < 100$	0.89577

TABLE IX
WFS' LOCATIONS OF DIFFERENT CASES

Case	WFs' locations (Bus No.)
1	9, 30, 63, 81, 91, 111 and 5
2	9, 30, 63, 81, 91, 111 and 38
3	9, 30, 63, 81, 91, 111 and 64
4	9, 30, 63, 81, 91, 111 and 71
5	9, 30, 63, 81, 91, 111 and 99
6	9, 30, 63, 81, 91, 111 and 116

the supply side. This is because there is little difference in regional carbon emission from the supply side. Also, it is hard to allocate the cost of RCEM from the supply side. Thus, a carbon flow tracing model proposed in [26] is applied to determine the regional carbon emission obligation from the demand side. The difference between the expected region carbon emission from both sides is depicted in Fig. 6. Table VII further proves the rational WFs' locations of Case 1 among the three cases. According to Fig. 6 and Table VII, the performance of different cases in controlling regional carbon emission from the supply side is almost the same. But from the demand side, WFs' location in Case 1 stands out. The results indicate that WFs should be installed in the region with heavier loads and higher carbon intensity TPGs, which can not only help decrease the total carbon emission but also prevent one of the regions from being polluted heavily.

VII. IEEE 118-BUS AND SHANGHAI CASE STUDIES

The RCEM model is solved for the IEEE 118-bus system [35] and a simplified Shanghai system to verify the feasibility of the proposed method in larger and actual systems here.

A. IEEE 118-Bus System

Table VIII gives the carbon intensities of generators used in 118-bus system. Six regions are distinguished covering nodes 1–24, 25–42, 43–65, 66–81, 82–100 and 101–118, respectively. Six cases of WFs' locations listed in Table IX are applied. All other parameters are set as the 30-bus case study above.

Table X gives the simulation results from both supply and demand sides. From the table, Case 3 has the best performance. So conclusions similar to the 30-bus case study are obtained. Adding WFs to the region with heavier loads is more conducive to balance regional carbon emission. Consequently, the proposed method can be also adopted in a larger system.

B. Simplified Shanghai System

A simplified Shanghai system provided by Shanghai Municipal Electric Power Company is applied in this part. The load and WFs' data are from May 1, 2013 in Shanghai. Six regions are distinguished based on the geographic locations, namely: 1, 2, 3, 4, 5, and 6.

Table XI gives the simulation results under different decisions with the same decision making condition as Table V. As all studies are done on the same system with WFs located in Region 5 which has the heaviest load, regional carbon emission

TABLE X
SIMULATION RESULTS OF 118-BUS SYSTEM UNDER DIFFERENT CASES FROM THE SUPPLY SIDE AND THE DEMAND SIDE ($L_{wi} = 1, i = 1,2,3, \alpha = \beta = 0.95$)

Case	Objective functions		Carbon emission in different regions [t]													
			Supply side							Demand side						
	$\bar{f}_1$[10^2\$]	$\bar{f}_2$[t]	$\bar{f}_3$[t]	1	2	3	4	5	6	$\bar{f}_3$[t]	1	2	3	4	5	6
1	14341	74359	39589	12337	12701	13943	14370	13443	7564	70374	14046	10358	19171	12028	11303	7454
2	14294	74116	47610	11886	11690	15953	14446	12028	8113	78080	14243	8963	19637	12760	10966	7548
3	14115	74318	37889	12395	12840	14403	14155	12595	7930	71182	14201	10222	19145	11923	11433	7394
4	14321	74500	36496	11764	12475	14436	13833	13424	8568	80268	14166	9197	20393	11914	11409	7422
5	14391	74298	43767	11815	12484	14239	15338	12355	8066	77211	13948	9175	19764	12883	10956	7571
6	14345	74304	38096	12298	12495	15561	12921	12677	8352	71627	14247	10133	18779	12657	11292	7195

TABLE XI
SIMULATION RESULTS OF SIMPLIFIED SHANGHAI SYSTEM UNDER DIFFERENT DECISIONS ($\alpha = \beta = 0.95$)

Decision	Objective functions		Carbon emission in different regions [t]													
			Supply side							Demand side						
	$\bar{f}_1$[\$]	$\bar{f}_2$[t]	$\bar{f}_3$[t]	1	2	3	4	5	6	1	2	3	4	5	6	
1	24767604	244353	164270	18847	44550	43593	42518	50283	44561	19436	41198	45703	29563	62953	45499	
2	24836824	244166	162012	19287	45070	43898	41882	49688	44341	19407	41219	45706	29513	62863	45458	
3	24736364	244553	163352	19882	44424	44468	41616	50657	43505	19492	41210	45717	29523	62987	45624	
4	24752388	244241	192714	16395	44507	44896	40420	50744	47279	19351	41212	45696	29494	62948	45540	
5	24866972	244195	144360	19425	44890	45088	43228	47097	44467	19413	41218	45703	29568	62873	45420	
6	24730040	244560	164882	19965	45007	44046	41380	50657	43505	19501	41209	45715	29524	62985	45627	
7	24712500	244356	203362	16911	43477	44842	42023	55406	41697	19325	41142	45753	29522	63149	45466	

differences from the demand side of different decisions are almost the same, 270000 t, not shown in the table. From the table, we can also find that f_3 varies greatly while f_1 and f_2 have less difference under different decisions. It indicates that the RCEM model can be used to reduce the emission of the region heavily polluted, such as Region 5. The cost allocation of RCEM can be done based on the region carbon emission of the supply side and demand side. So the proposed RCEM model can not only be adopted in the actual system, but also have a promising future.

VIII. CONCLUSIONS

A new multi-objective RCEM model combining PPF with correlated random variables is proposed in this paper. Different from the traditional ones, a new objective called region carbon emission difference is added to control equilibrium degree of contamination. From the simulation results, relevant conclusions can be drawn as follows:

1. The correlations do affect the moments of the WFs' output. Higher correlation coefficients lead to larger standard deviations of WFs' output. But the WFs have nearly the same expected output when the correlation coefficient is 0 or 1.
2. Cornish-Fisher has better performance in approximating the real distribution than Gram-Charlier for PPF problem with the non-Gaussian PDF.
3. With the increase in confidence levels, the value of the three objectives will rise for more stringent constraints which need to be satisfied.
4. Flexible reference membership values make this model a useful carbon emission management tool for system operators.
5. WFs should be installed in the region with heavy loads and high carbon intensity TPGs which can help reduce carbon intensity from both supply and demand side.

In conclusion, as the RCEM model can be adopted in both test and actual systems, it provides a useful tool to manage the regional carbon emission inside a city and evaluate the rationality of the regional grid planning with wind power.

REFERENCES

[1] *Climate Change 2007: Synthesis Report*, Intergovernmental Panel on Climate Change, IPCC Plenary XXVII, Valencia, Spain, 2007 [Online]. Available: http://www.ipcc.ch/pdf/assessment-report/ar4/syr/ar4_syr_spm.pdf

[2] Q. Chen, C. Kang, Q. Xia, and J. Zhong, "Power generation expansion planning model towards low-carbon economy and its application in China," *IEEE Trans. Power Syst.*, vol. 25, no. 2, pp. 1117–1125, May 2010.

[3] T. Logenthiran, D. Srinivasan, and T. Z. Shun, "Demand side management in smart grid using heuristic optimization," *IEEE Trans. Smart Grid*, vol. 3, no. 3, pp. 1244–1252, Sep. 2012.

[4] S. H. Madaeni and R. Sioshansi, "Using demand response to improve the emission benefits of wind," *IEEE Trans. Power Syst.*, vol. 28, no. 2, pp. 1385–1394, May 2013.

[5] E. Denny and M. O'Malley, "Wind generation, power system operation, and emissions reduction," *IEEE Trans. Power Syst.*, vol. 21, no. 1, pp. 341–347, Feb. 2006.

[6] Q. Chen, C. Kang, Q. Xia, and D. S. Kirschen, "Optimal flexible operation of a CO_2 capture power plant in a combined energy and carbon emission market," *IEEE Trans. Power Syst.*, vol. 27, no. 3, pp. 1602–1609, Aug. 2012.

[7] S. Lu, S. Lou, Y. Wu, and X. Yin, "Power system economic dispatch under low-carbon economy with carbon capture plants considered," *IET Gener., Transm. Distrib.*, vol. 7, no. 9, pp. 991–1001, Sep. 2013.

[8] Z. Li, Q. Guo, H. Sun, Y. Wang, and S. Xin, "Emission-concerned wind-EV coordination on the transmission grid side with network constraints: Concept and case study," *IEEE Trans. Smart Grid*, vol. 4, no. 3, pp. 1692–1704, Sep. 2013.

[9] C. Wang, Z. Lu, and Y. Qiao, "A consideration of the wind power benefits in day-ahead scheduling of wind-coal intensive power systems," *IEEE Trans. Power Syst.*, vol. 28, no. 1, pp. 236–245, Feb. 2013.

[10] B. Borkowska, "Probabilistic load flow," *IEEE Trans. Power App. Syst.*, vol. PAS-93, no. 3, pp. 752–759, May 1974.

[11] J. F. Dopazo, O. A. Klitin, and A. M. Sasson, "Stochastic load flows," *IEEE Trans. Power App. Syst.*, vol. 94, pp. 299–309, Mar. 1975.

[12] X. Li, Y. Li, and S. Zhang, "Analysis of probabilistic optimal power flow taking account of the variation of load power," *IEEE Trans. Power Syst.*, vol. 23, no. 4, pp. 992–999, Aug. 2008.

[13] A. R. Malekpour, T. Niknam, A. Pahwa, and A. K. Fard, "Multi-objective stochastic distribution feeder reconfiguration in systems with wind power generators and fuel cells using the point estimate method," *IEEE Trans. Power Syst.*, vol. 28, no. 2, pp. 1483–1492, May 2013.

[14] J. M. Morales, L. Baringo, A. J. Conejo, and R. Minguez, "Probabilistic power flow with correlated wind sources," *IET Gener., Transm. Distrib.*, vol. 4, no. 5, pp. 641–651, May 2010.
[15] J. M. Morales and J. Pérez-Ruiz, "Point estimate schemes to solve the probabilistic power flow," *IEEE Trans. Power Syst.*, vol. 22, no. 4, pp. 1594–1601, Nov. 2007.
[16] G. Verbič and C. A. Cañizares, "Probabilistic optimal power flow in electricity markets based on a two-point estimate method," *IEEE Trans. Power Syst.*, vol. 21, no. 4, pp. 1883–1893, Nov. 2006.
[17] H. Yu, C. Y. Chung, K. P. Wong, H. W. Lee, and J. H. Zhang, "Probabilistic load flow evaluation with hybrid Latin hypercube sampling and Cholesky decomposition," *IEEE Trans. Power Syst.*, vol. 24, no. 2, pp. 661–667, May 2009.
[18] Y. Yuan, J. Zhou, P. Ju, and J. Feuchtwang, "Probabilistic load flow computation of a power system containing wind farms using the method of combined cumulants and Gram-Charlier expansion," *IET Renewable Power Gener.*, vol. 5, no. 6, pp. 448–454, Nov. 2011.
[19] P. Zhang and S. T. Lee, "Probabilistic load flow computation using the method of combined cumulants and Gram-Charlier expansion," *IEEE Trans. Power Syst.*, vol. 19, no. 1, pp. 676–682, Feb. 2004.
[20] Y. Chen, J. Wen, and S. Cheng, "Probabilistic load flow method based on Nataf transformation and Latin Hypercube Sampling," *IEEE Trans. Sustainable Energy*, vol. 4, no. 2, pp. 294–301, Apr. 2013.
[21] P. Sauer and G. Heydt, "A convenient multivariate Gram-Charlier Type A series," *IEEE Trans. Commun.*, vol. 27, no. 1, pp. 247–248, Jan. 1979.
[22] R. N. Allan, A. M. Leite de Silva, and R. C. Burchett, "Evaluation methods and accuracy in probabilistic load flow solutions," *IEEE Trans. Power App. Syst.*, vol. PAS-100, no. 5, pp. 2539–2546, May 1981.
[23] J. Usaola, "Probabilistic load flow with wind production uncertainty using cumulants and Cornish-Fisher expansion," *Electr. Power Energy Syst.*, vol. 31, no. 9, pp. 474–481, Oct. 2009.
[24] F. J. Ruiz-Rodriguez, J. C. Hernandez, and F. Jurado, "Probabilistic load flow for photovoltaic distributed generation using the Cornish-Fisher expansion," *Elect. Power Syst. Res.*, vol. 89, pp. 129–138, Aug. 2012.
[25] G. W. Hill and A. W. Davis, "Generalized asymptotic expansions of Cornish-Fisher type," *The Annals of Mathematical Statistics*, vol. 39, no. 4, pp. 1264–1273, 1968.
[26] B. Li, Y. Song, and Z. Hu, "Carbon flow tracing method for assessment of demand side carbon emission obligation," *IEEE Trans. Sustain. Energy*, vol. 4, no. 4, pp. 1100–1107, Oct. 2013.
[27] Y. Ou and C. Singh, "Assessment of available transfer capability and margins," *IEEE Trans. Power Syst.*, vol. 17, no. 2, pp. 463–468, May 2002.
[28] K. Xie and R. Billinton, "Considering wind speed correlation of WECS in reliability evaluation using the time-shifting technique," *Electr. Power Syst. Res.*, vol. 79, no. 4, pp. 687–693, Apr. 2009.
[29] L. N. de Castro and F. J. Von Zuben, "Learning and optimization evolutionary computation," *IEEE Trans. Evol. Comput.*, vol. 6, no. 3, pp. 239–251, Jun. 2002.
[30] Y.-L. Chen and C.-C. Liu, "Interactive fuzzy satisfying method for optimal multi-objective VAR planning in power systems," *IEE Proc., Gen., Transm., Distrib.*, vol. 141, no. 6, pp. 554–560, Nov. 1994.
[31] O. Alsac and B. Stott, "Optimal load flow with steady state security," *IEEE Trans. Power Syst.*, vol. PAS-93, no. 3, pp. 745–751, May 1974.
[32] R. W. Ferrero, S. M. Shahidehpour, and V. C. Ramesh, "Transaction analysis in deregulated power system using game theory," *IEEE Trans. Power Syst.*, vol. 12, no. 3, pp. 1340–1347, Aug. 1997.
[33] M. Fan, V. Vittal, G. T. Heydt, and R. Ayyanar, "Probabilistic power flow analysis with generation dispatch including photovoltaic resources," *IEEE Trans. Power Syst.*, vol. 28, no. 2, pp. 1797–1805, May 2013.
[34] A. Steiner, "Fitting non-normal distributions with calibrated Cornish-Fisher expansions," Jun. 30, 2013 [Online]. Available: http://ssrn.com/abstract=2287543
[35] *Index of /Data* [Online]. Available: http://motor.ece.iit.edu/data

Xu Wang received the B.S. degree in electrical engineering from Southeast University, Nanjing, China, in 2010. Currently, he is pursuing the Ph.D. degree in the School of Electronic Information and Electrical Engineering, Shanghai Jiao Tong University, Shanghai, China.

Yu Gong received the B.S. degree in electrical engineering from Shanghai Jiao Tong University, Shanghai, China, in 2012. Currently, he is pursuing the M.S. degree in the School of Electronic Information and Electrical Engineering, Shanghai Jiao Tong University, Shanghai, China.

Chuanwen Jiang received the M.S. and Ph.D. degrees from Huazhong University of Science and Technology, Wuhan, China, in 1996 and 2000, respectively, and completed his postdoctoral research in the School of Electronic Information and Electrical Engineering, Shanghai Jiao Tong University, Shanghai, China, in 2002.

He is a Professor with the School of Electronic Information and Electrical Engineering, Shanghai Jiao Tong University. He is currently researching reservoir dispatch, load forecast in power systems, and the electrical power market.